JAXA-ONERA-DLR COOPERATION: RESULTS FROM ROTOR OPTIMIZATION IN HOVER

Gunther Wilke, gunther.wilke@dlr.de, German Aerospace Center/DLR (Germany)
Joëlle Bailly, joelle.zibi@onera.fr, The French Aerospace Lab/ONERA (France)
Keita Kimura, keita.kimura@jaxa.jp, Japan Aerospace Exploration Agency/JAXA (Japan)
Yasutada Tanabe, tan@chofu.jaxa.jp, Japan Aerospace Exploration Agency/JAXA (Japan)

Abstract
A cooperation on the aerodynamic optimization of helicopter rotors has been formed by JAXA, ONERA and DLR. This work represents the conclusions drawn from the first phase: optimization of a hovering rotor. The HART-II blade is first investigated with low-fidelity tools and compared against state-of-the art CFD simulations. Following up on this, the HART-II blade chord distribution and twist are optimized with the low-fidelity tools as well as CFD. Due to observed differences in the outcome of the CFD simulations for the low-fidelity optimized blades by the partners, a deeper investigation of the effects of the turbulence modelling approach, elasticity and grid topology is undertaken. The outcome is that the chosen flight condition is close to thrust of the maximum Figure of Merit and the vortex triggered separation on the outboard sections of the blade has to be modelled correctly. In this study, the blade grids had the most noticeable effect on the results, followed by the turbulence model and elasticity. With respect to the optimization, care must be taken when optimizing with low-fidelity methods, whereas CFD optimized blades were found to lead to more robust designs even though they have only been optimized for a single point. Reason is the more accurate modelling of the stall phenomenon with respect to geometrical changes.

1. INTRODUCTION

The flow around helicopter rotor blades is of complex nature, due to the vortex-dominated flow and the various speed regimes blade sections undergo. Thus, the correct simulation of the rotor aerodynamics is a challenging task. Trying to improve current rotor blade designs through numerical optimization to reduce power requirements becomes even more challenging as often many simulations are required to arrive at an improved design.

The three research organizations of JAXA, ONERA and DLR decided to join forces in June 2019 to tackle these challenges together. The focus lies on the comparison and investigation of the aerodynamic and aero-acoustic optimization and simulation strategies employed by each partner with the goal to improve the optimization processes and the obtained designs themselves.

Looking at the past endeavours, JAXA has successfully optimized rotor blades for a compound helicopter [1] and has worked already collaboratively with DLR on the accurate flow simulation of rotor blades [2]. JAXA and ONERA previously had a cooperation, where rotor blades have been optimized in hover and forward flight [3]. ONERA and DLR have an even longer history of working together and the ERATO rotor is one example [4]. More recently, work has been done on the RACER compound helicopter [5]. Therefore, it was natural to set up a tri-lateral cooperation.

As opposed to a gradient based optimization using the adjoint method as for example used by Fabiano and Mavripilis [6], Wang et al. [7] or Fitzgibbon [8], in this cooperation a surrogate based optimization approach is analysed [9]. In the first phase of the cooperation, an optimization with five design variables driving the chord and twist distributions of the rotor is carried out, minimizing the required power, albeit Figure of Merit, of the HART-II rotor [10] in hover. A first paper on that matter has been presented [11], which primarily focused on low fidelity results with first CFD based results for the baseline rotor.

In this paper, the different outcomes from the low fidelity and high-fidelity optimizations are investigated, as well as the effects on different turbulence modelling, grid topologies and the inclusion of elasticity are investigated.

2. METHODOLOGY

2.1. Low-Fidelity Setups

The underlying methodology used for the low-fidelity aerodynamics is the blade-element theory (BET). The sectional forces of the rotor blades are determined from look-up tables of the airfoils. The main differences lie in the inflow model used by the partners. JAXA utilizes the momentum theory (BEMT), while DLR and ONERA utilized a finite-state model based on the work by Peters et al. [12] and implemented by Basset et al. [13] into the comprehensive code HOST [14].

Presented at 47th European Rotorcraft Forum, Virtual, United Kingdom, 7-10 September, 2021
This work is licensed under the Creative Commons Attribution International License (CC BY). Copyright © 2021 by author(s).

Since both types of inflow models do not feature any tip-vortex modelling, a simple cut-off factor is used as it was found to work better than Prandtl's tip-loss function. The setups are briefly summarized in Table 1.

Table 1: Summary of Low-Fidelity Models. Polynomials refers to the number of Legendre polynomials used for the radial representation in the finite state model.

	JAXA	ONERA	DLR
code	rBEMT	HOST	
Inflow model	Momentum Theory	Finite state	
Polynomials		24	8
Structural adjustment	-	Polynomial fit [15]	Linear scaling [16]

Table 2: CFD solvers & settings.

	JAXA	ONERA	DLR
solver	rFlow3D [17]	*elsA* [18]	FLOWer [19]
Inviscid scheme	4thorder FMCT + SLAU2 [20] [21]	2nd order JST [22]	4th order FMCT (vA) + SLAU2 [23] [24]
	with 2nd order finite volume metrics		
Time integration	Dual time LU-SGS & 4 stage RK [25] [26]	Backward Euler scheme + LU-SGS (steady)	Dual time 5 stage RK + impl. res. smooth. & multigrid [27]
Turb. model	SA-R Fully turbulent [28] [29]	Kok-SST Fully turbulent [30]	SA-R + empirical transition or Menter SST fully turbulent [28] [29] [31] [32]
Rotor motion	Rigid	Elastic, through delta airloads approach [33] with HOST	

2.2. Computational Fluid Dynamics

All three partners utilize block-structured codes for the simulation of the rotor flows. For brevity, the major features are compared in Table 2. For more information, please consult the associated references.

2.3. Grid Topology and Generation

Since the partners use different meshing tools and CFD codes, it has been difficult to run common setups. However, a minimum quality guideline was agreed upon, as an attempt to ensure sufficiently matching results. The most mandatory one was a y^+ spacing of the first cell of 1, while in chord- and spanwise direction at least 80 cells needed to be deployed with roughly 35 cells in the boundary layer.

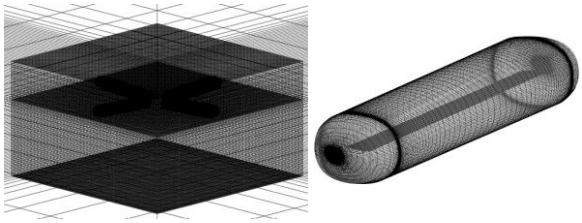

JAXA (chimera, 2 backgrounds + blade)

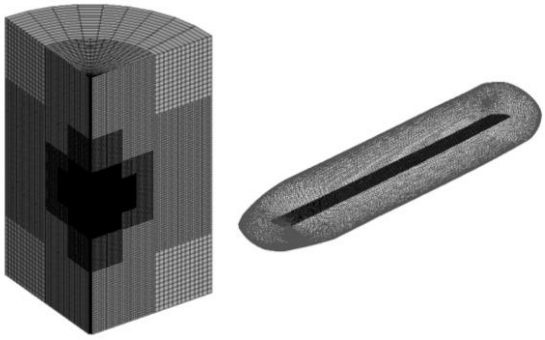

ONERA (chimera, 1/4 periodic BK + blade)

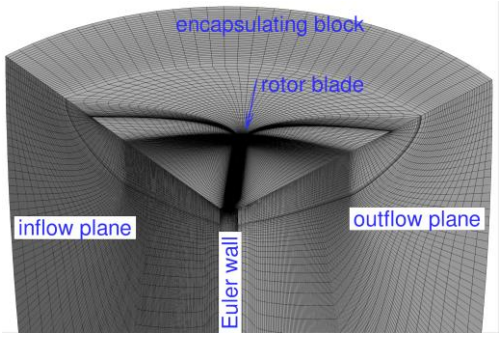

DLR (split in the middle)

Figure 1: Concept sketches of grids [11].

For JAXA, a baseline grid is prepared with Pointwise [34], which is then deformed during the optimization to realize the various geometries investigated. The whole rotor is embedded into two sets of background grids, an inner grid with a higher point density, and

This work is licensed under the Creative Commons Attribution International License (CC BY). Copyright © 2021 by author(s).

an outer grid that extends to the farfield boundaries to reduce potential reflections.

Table 3: Grid properties of each partner's mesh.

	JAXA	ONERA	DLR
blade mesh cells			
Chordwise	160	80	160
Spanwise	120	80	160
Boundary layer	~50	~35	~35-60
Wake resolution (in % chord length)			
Circumferential			9-100
Radial	20	7	9
vertical			13
Farfield/Outer grids dimensions (in rotor radii)			
Vertical	100	6	6
Lateral	100	6	2.5
Total # of cells	16M	6.7M	4.4M
Full rotor equivalent	16M	26.8M	17.6M

The ONERA takes a similar approach, but models a single rotor blade within a quarter cylinder using the Chimera technique. A multi-block, deformable mesh of O-H type is generated for the blade mesh, where the root and tip cap are made of separate grid blocks. The grids of the new rotor designs are generated through a deformation of the baseline grid, based on a quaternion approach [35], developed in the in-house QUANTUM code. The background grid is automatically generated using Cassiopee [36], a set of Python modules for pre- and post-processing of CFD computations. The Froude boundary condition is applied to correct the inflow at the farfield through a source/sink model based on the rotor thrust.

DLR uses the in-house grid generator G^3 based on transfinite interpolation, like GEROS [37]. Thus, a new grid is automatically generated for each new rotor design. Here an O-O block is generated with periodic boundaries, which is extended by additional H-O blocks towards the farfield. Like ONERA, the Froude boundary condition is utilized on the outer mesh.

In Figure 1, sketches of the individual meshes are given, while in Table 3 a comparison of grid numbers is given.

It is noteworthy that JAXA thus has a Cartesian background grid, while ONERA has a mesh in polar coordinates and DLR blends over from the blade mesh towards the periodic boundaries. This enables DLR to use the least grid points at the cost of skewed cell regions. Multiplying the ONERA and DLR grids by four to complete the rotor shows that the ONERA grid would have the most grid points, while JAXA and DLR would have comparable number of grid points.

2.4. Optimization Framework

The general optimization approach for this work is based on the EGO optimization algorithm by Jones et al. [38]. A Kriging surrogate model is built after an initial data sampling and the next infill point is sought using the maximum expected improvement. However, variations in the implemented frameworks exist and are listed in Table 1.

Table 4: Optimization Frameworks.

	JAXA	ONERA	DLR
Frame-work	[39] [40]	KORRIGAN [41]	POT [9]
Meta model	Kriging	Co-Kriging [42]	Hierarchical Kriging [43]
Opti-mizer	Genetic Algorithm [44] [45]		Diff. Evolution + Nelder & Mead [46] [47]

The low-fidelity optimizations are purely carried out with the standard Kriging model. For the high-fidelity optimizations, ONERA and DLR make use of the variable-fidelity approach, where the Kriging model is augmented with high-fidelity data. ONERA utilizes the low-fidelity model based on the finite-state inflow for Kriging combined with high fidelity data obtained from CFD/CSD coupling for Co-Kriging. DLR generates CFD data using a factor eight coarsened grid and Hierarchical Kriging.

3. OPTIMIZATION TASK

For this study, the HART-II rotor is selected as the reference as it is well documented with openly available data [10] and features a simple geometry. The baseline test environment is copied over, yet the rotor is placed in a hover condition with a set thrust equivalent to $c_T/\sigma = 0.1$, which is trimmed with collective pitch. The according thrust is referred to as the design thrust in this paper.

The goal function in this study is the maximization of the Figure of Merit defined as

$$FM = \frac{c_T^{1.5}}{\sqrt{2}c_Q}$$

With c_T and c_Q being the thrust and torque coefficients of the rotor. Since the rotor is trimmed to

This work is licensed under the Creative Commons Attribution International License (CC BY). Copyright © 2021 by author(s).

a set thrust, this is the same as minimization of the required power.

A total of five design parameters is utilized: three chord and two twist parameters. The parameterization description is done through cubic splines. The chord distribution is set up with respect to the reference chord length c_{ref} of 0.121m and is scaled afterwards to match the thrust weighted solidity of the HART-II rotor. The twist spline is applied in the Δ-form meaning it is added to the existing linear twist with a gradient of -8˚/R. The design variables and their limits are listed in Table 5 with a sketch given in Figure 2.

Table 5: Design variables.

variable	location	limits
$\Delta\theta_1$	87.5% r/R	±5˚
$\Delta\theta_2$	100% r/R	-10˚~0˚
r_c	-	65~85% r/R
$chord_1$	$r=r_c$	1.0~1.5 c_{ref}
$chord_2$	100% r/R	0.5-1.0 c_{ref}

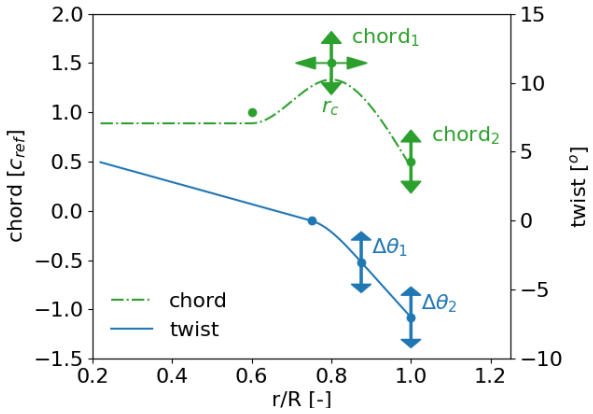

Figure 2: Sketch of design variables.

4. BASELINE RESULTS

As a first measure, the results for the chosen baseline rotor are presented, which is also a recapitulation of the previous paper [11]. In Figure 3 and Figure 4, the Figure of Merit polars of the low-fidelity and CFD simulations are plotted, respectively. The DLR CFD simulations are split into SA-LT and SST-FT, which refer to the application of the SA turbulence model with laminar turbulent transition prediction and the Menter SST model in fully turbulent mode. While the rough estimate for the Figure of Merit at design thrust can be replicated with the low-fidelity models, the functional behaviour is better replicated by the CFD simulations with respect to the experimental data. Also, the variation among the partners' results is lower for the CFD simulations. Since the here employed turbulence models are not suited for large separations, the second point past the maximum Figure of Merit is not included in the curve fit anymore and only given as a scatter point.

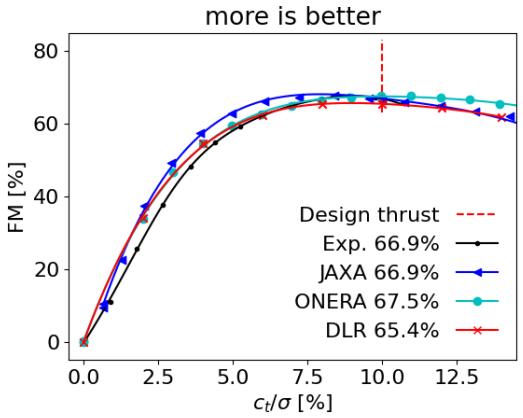

Figure 3: Figure of Merit polar of HART-II rotor for the low-fidelity methods. Experimental data from [48].

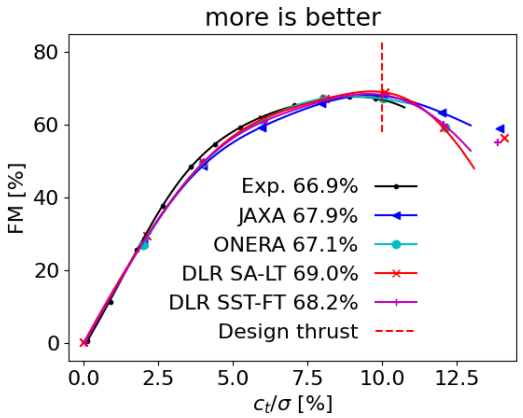

Figure 4: Figure of Merit polar of HART-II rotor for the CFD simulations. Experimental data from [48].

Going into more detail, the according normal load distributions at the design thrust are found in Figure 5 and Figure 6. From comparison of the low-fidelity results with the CFD data, it is seen that the shape towards the blade tip past (r/R > 80%) shows a significantly different perception between the two general approaches. The low-fidelity methods capture a mostly linear trend and then drop off at the cut-off value from the tip loss factor. For the CFD based methods, the added lift from the upwash from the blade tip vortex of the previous blade shows an increase in the lift gradient, which then drops off at the tip due to the current blades tip vortex. Comparing the individual loads among the partners, minor differences are noticed, which are acceptable given the here applied mesh resolution.

This work is licensed under the Creative Commons Attribution International License (CC BY). Copyright © 2021 by author(s).

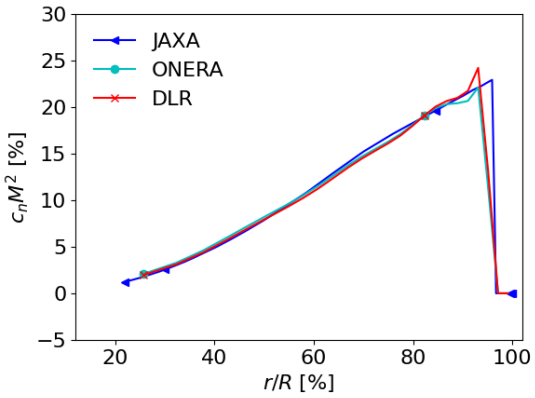

Figure 5: normal load distribution of HART-II rotor for low-fidelity methods at design thrust.

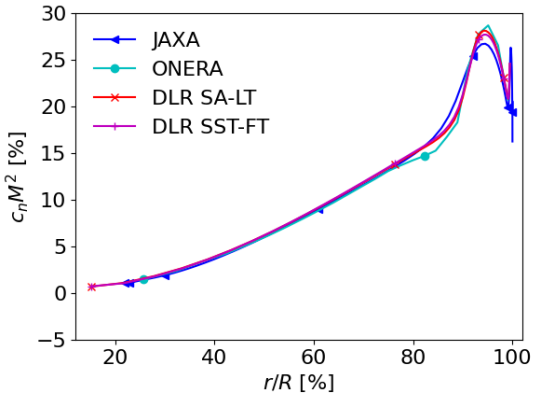

Figure 6: normal load distribution of HART-II rotor for CFD simulations at design thrust.

In Figure 7 the pressure distribution for a radial cut at r/R=95% is plotted for the design thrust condition. Only minor differences are observed in the suction peak. The suction peak of the ONERA results is closest to the leading edge, whereas JAXA's suction peak is furthest away with the DLR results in between. The reason why this cut has been selected is that it is in the upwash area of the previous tip vortex and a stronger tip vortex causes higher suction peaks. See Figure 8 for a comparison of the vortex conservation of the individual grids. Since JAXA employed the largest grid spacing in the background, there is a volume jump from the blade grid to the background grid in the interpolation area, the strength is the least well conserved, thus shifting the suction peak further downstream.

In Figure 9 the skin friction distributions retrieved for the r/R=95% cut are plotted for each partner's CFD result. JAXA's skin friction is overall higher than the skin friction seen by ONERA and DLR. For all partners, the skin friction dips at a small area just before x/c ≈ 20% on the suction side. This is mostly pronounced for DLR's laminar turbulent simulation, followed by DLR's fully turbulent and JAXA's fully turbulent simulations and is least pronounced for ONERA's simulation.

These skin friction plots on the one hand allow the assessment on how much viscosity is added by the different turbulence models, but on the other hand help identify regions of separation. While strictly speaking, a negative skin friction coefficient is just an indication for reverse flow, it is synonymously treated as the occurrence of separated flow, here. This seems to be sufficiently valid for this cut and flight condition. Looking at Figure 10, where the skin friction distribution is plotted over a range of thrusts, and the associated velocity fields for the two higher thrusts in Figure 11, it is seen that the separation builds up roughly behind the suction peak for growing thrusts until it is fully separated for the highest thrust. While at first, this is just a small bubble, which is barely noticed in the velocity plot of the design thrust c_T/σ=10% and is represented by the dip of the skin friction coefficient below zero, the larger part of the upper surface is separated for c_T/σ=12%, which coincides with the larger area of skin friction below zero. Opposing this, at c_T/σ=6%, no sign of the build-up is seen and therefore it is assumed that the tip vortex is too weak in this condition to show an impact on the skin friction distribution yet. Please note that the skin friction dip at x/c ≈ 95% comes from the airfoil geometry, which transitions from the original NACA23012 airfoil to the tab geometry.

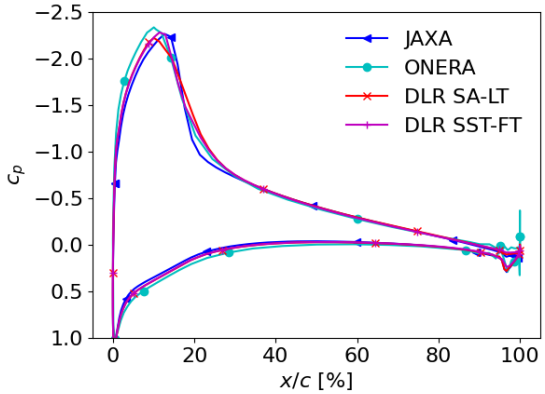

Figure 7: pressure distribution of the HART-II rotor @ r/R=95% and design thrust.

This work is licensed under the Creative Commons Attribution International License (CC BY). Copyright © 2021 by author(s).

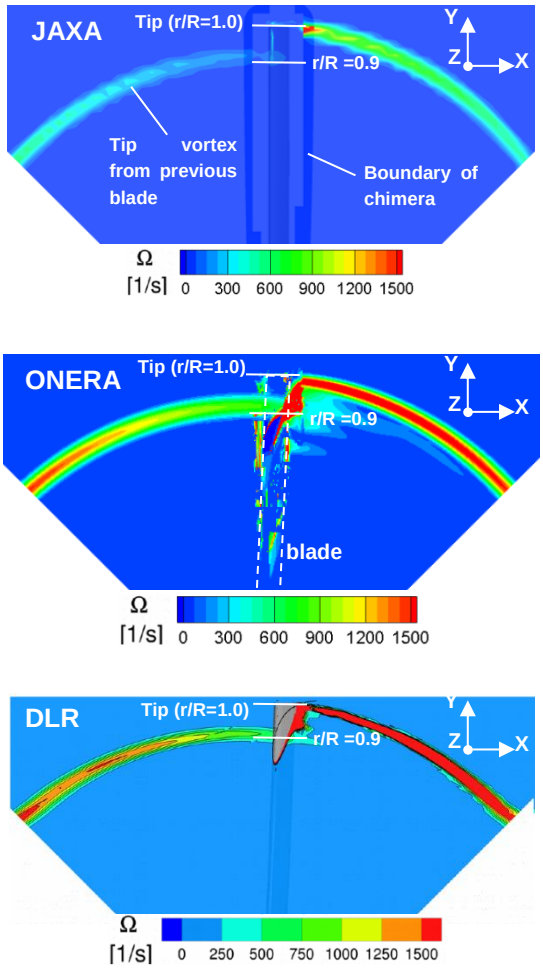

Figure 8: Vorticity plots of HARTII CFD simulations by the individual partners. Cut through the thrust axis 0.1m above the rotor center. From [11].

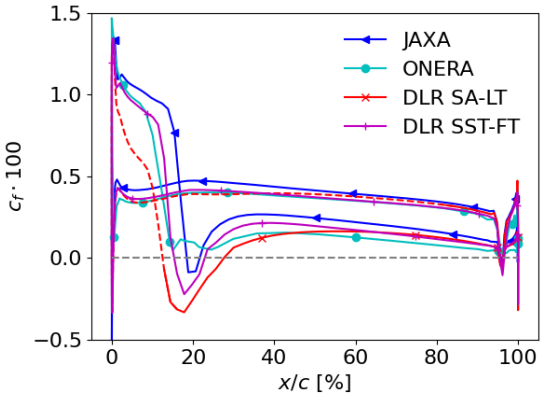

Figure 9: skin friction distribution of the HART-II rotor @ r/R = 95% and design thrust. Dashed lines mark laminar regions.

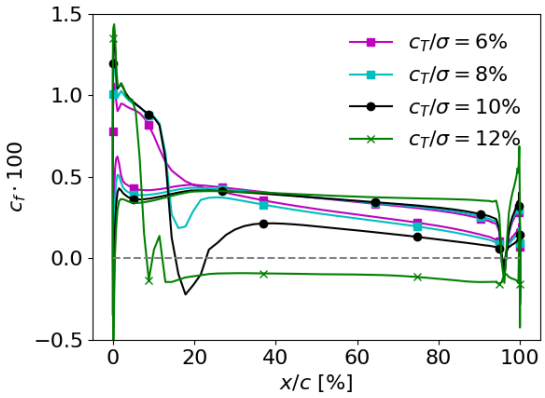

Figure 10: skin friction distribution of the HART-II rotor @ r/R = 95% and various thrusts for DLR SST FT simulations. Dashed lines mark laminar regions.

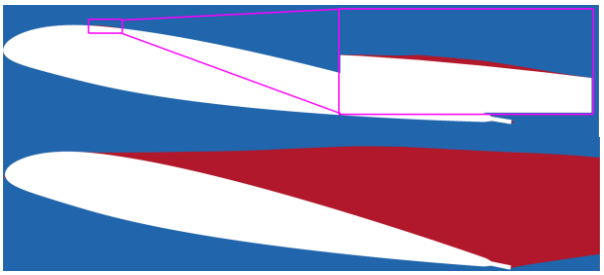

Figure 11: Velocity plots at r/R=95% for the HART-II rotor. Top: c_T/σ = 10%, bottom c_T/σ = 12%. Blue: forward flow, Red: reversed flow.

5. LOW-FIDELITY OPTIMIZED BLADES

The distribution of parameters of the low-fidelity optimized blades are plotted in Figure 12 for the chord and Figure 13 for the twist parameters. The agreement among the chord parameters is very high, while differences between the twist parameter, especially at the tip are visible. JAXA features the steepest twist gradient with an offset of $\Delta\theta_2$ = -8.1˚ whereas as the ONERA blade has a $\Delta\theta_2$ = -3.3˚ and the DLR blade in between with $\Delta\theta_2$ = -5.7˚. Even though DLR and ONERA apply the same comprehensive code, it is found that the number of radial harmonics employed in the finite state model has a small impact on the solution explaining the differences between the DLR and ONERA blade.

With respect to the Figure of Merit of these blades reported by the individual partners, they all improve noticeably over the reference blade when computed with the low-fidelity methods, refer to Figure 14 to Figure 16. It comes to no surprise that the individual blades by each partner are the best when evaluated with the methods they have been optimized with except for JAXA, where the DLR blade is slightly better. JAXA reports the largest gain of Figure of

This work is licensed under the Creative Commons Attribution International License (CC BY). Copyright © 2021 by author(s).

Merit of the new blades, whereas ONERA the smallest.

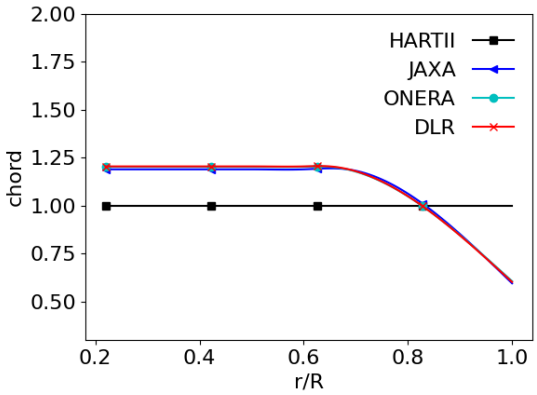

Figure 12: chord distribution of low-fidelity optimized blades.

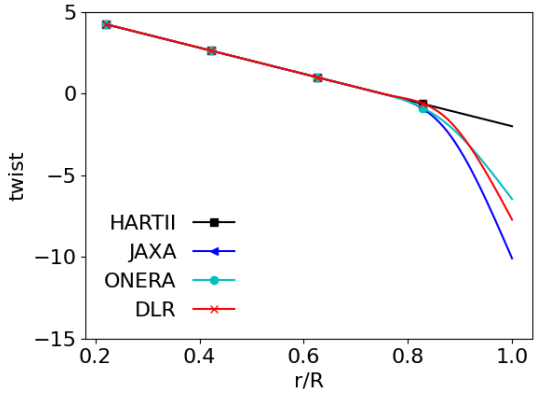

Figure 13: Twist distribution of low-fidelity optimized blades.

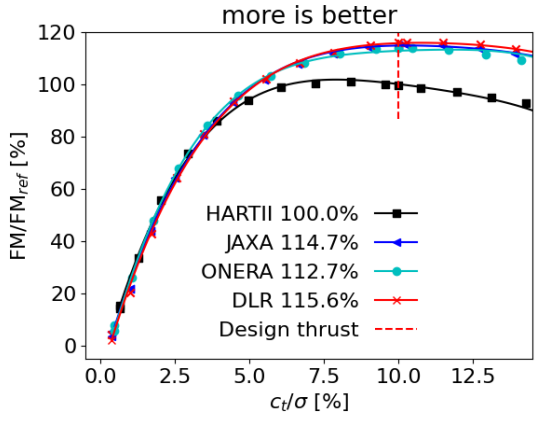

Figure 14: Figure of Merit polars for low-fidelity optimized blades computed by JAXA's low-fidelity approach.

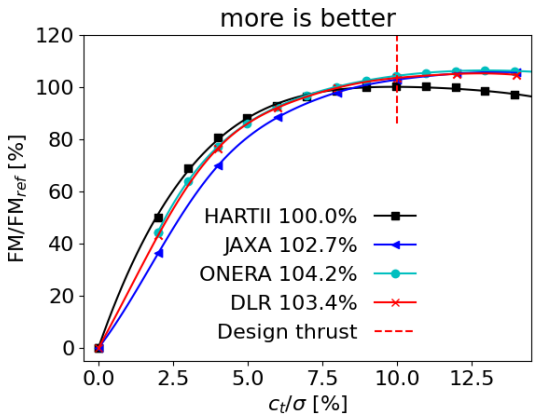

Figure 15: Figure of Merit polars for low-fidelity optimized blades computed by ONERA's low-fidelity approach.

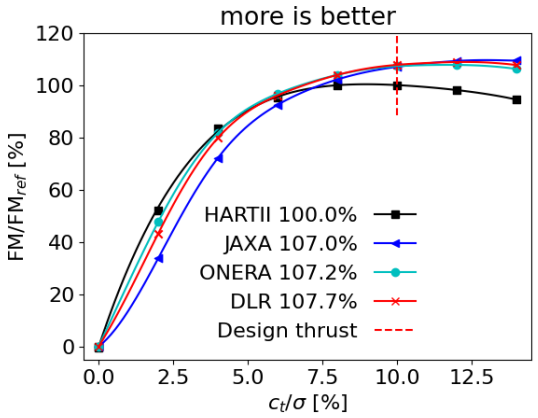

Figure 16:Figure of Merit polars for low-fidelity optimized blades computed by DLR's low-fidelity approach.

A cross-examination of all these blades is undertaken by each partner with their CFD methods to assess the gains achieved with a high-fidelity approach and to see how far the spread is among the partners for resolving individual rotor geometries.

The Figure of Merit polars computed by JAXA are shown in Figure 17, by ONERA in Figure 18 and by DLR in Figure 19. The actual values are scaled with the Figure of Merit of the HARTII-reference blade at design thrust reported by each partner's CFD code to better visualise the gains of each blade. It is noteworthy, that for JAXA and DLR, all low-fidelity blades improve over the HART-II blade. The prediction with laminar-turbulent transition by DLR shows greater gains than those seen from DLR's fully turbulent simulations. These results are closer together with JAXA's fully turbulent results, even though the gains are generally a bit higher for DLR. Also, the ranking of blades is then similar to JAXA, where JAXA's blade performs best due to the high outboard twist, followed by DLR's and ONERA's

This work is licensed under the Creative Commons Attribution International License (CC BY). Copyright © 2021 by author(s).

blade in descending order of the (negative) outboard twist. Opposing this, the ONERA results only show a mild improvement for the JAXA blade, while the DLR blade deteriorates and the ONERA blade drastically deteriorates over the baseline blade. When excluding the HART-II blade, the ranking among the blades remains the same, nevertheless, this is an unexpected outcome.

In order to obtain a better understanding between the differences of JAXA and DLR results with those by ONERA, the skin friction plots are studied in Figure 21 to Figure 24 for the various simulations. For the JAXA simulations, the ONERA blade features the overall highest skin friction due to the fact that the dip at the suction side at x/c ≈ 20% is very small in contrast to the dips by the other blades. Moving onto the ONERA results, the impact of the dip is resolved differently. For the ONERA blade, it drops down at x/c ≈ 15% and does not recover from this low value, being an indication for detached flow. Upon checking the flow simulation, it is confirmed that a strong separation is in place for this blade coming from the upwash of the tip vortex of the previous blade at this radial location. The effect is less pronounced for the DLR blade, and even less for the JAXA blade, yet still stronger than for the HART-II rotor. This explains the sudden overall reduced performance of the low-fidelity optimized blade for the ONERA simulations. Moving onto the two DLR setups, the small dips at x/c ≈ 20% are given for all blades and are of similar magnitude. An exception is the JAXA blade for the SST fully turbulent (FT) simulation, where it is a little bit reduced, which also explains the greater gain in Figure of Merit over the other blades when using this turbulence model setup.

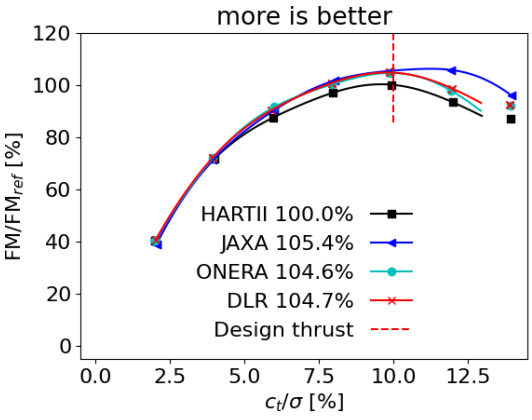

Figure 17: Figure of Merit polars for low-fidelity optimized blades computed by JAXA's CFD approach.

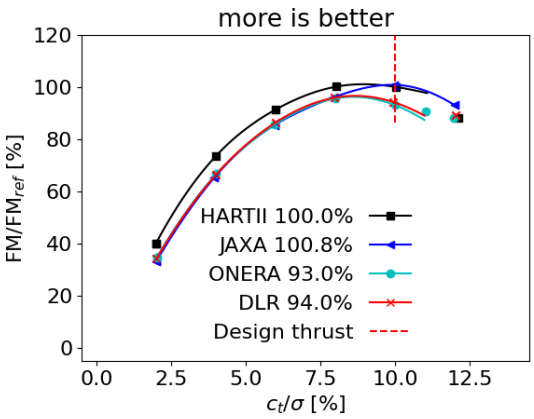

Figure 18: Figure of Merit polars for low-fidelity optimized blades computed by ONERA's CFD approach.

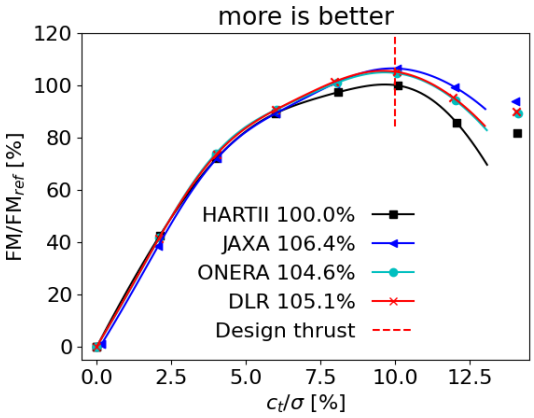

Figure 19: Figure of Merit polars for low-fidelity optimized blades computed by DLR's CFD approach (SA-R LT).

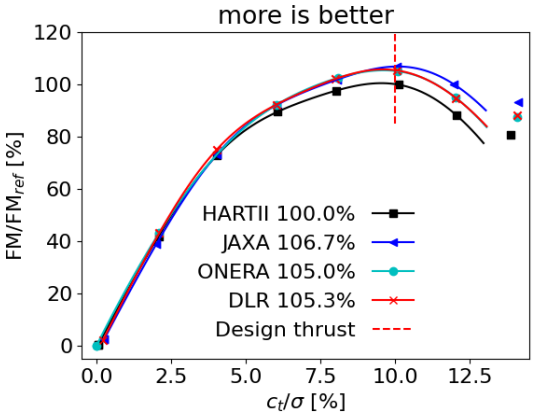

Figure 20: Figure of Merit polars of low-fidelity optimized blades computed by DLR's CFD approach (SST FT).

This work is licensed under the Creative Commons Attribution International License (CC BY). Copyright © 2021 by author(s).

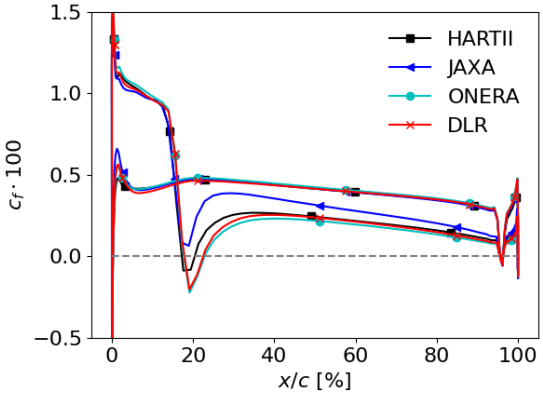

Figure 21: Skin friction distribution of low-fidelity optimized blades @ r/R = 95% and design thrust for JAXA's CFD simulations.

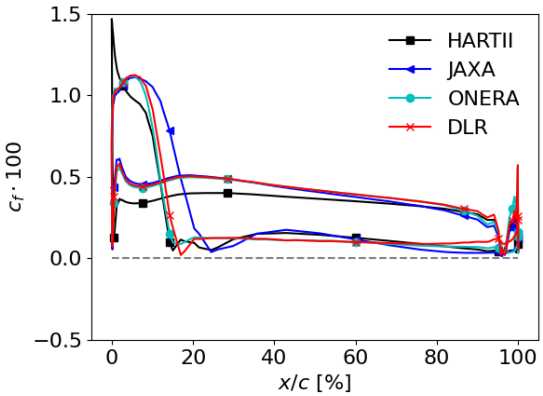

Figure 22: Skin friction distribution of low-fidelity optimized blades @ r/R = 95% and design thrust for ONERA's CFD simulations.

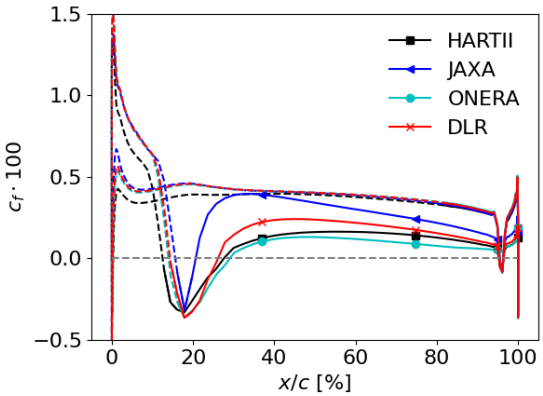

Figure 23: Skin friction distribution of low-fidelity optimized blades @ r/R = 95% and design thrust for DLR's CFD (SA-R LT) simulations. Dashed lines mark laminar regions.

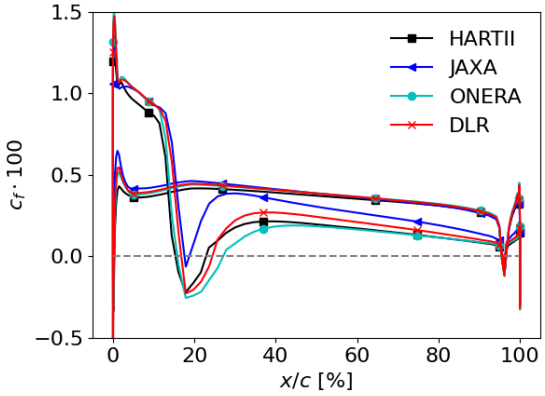

Figure 24: : Skin friction distribution of low-fidelity optimized blades @ r/R = 95% and design thrust for DLR's CFD (SST FT) simulations.

6. IMPACT OF NUMERICAL MODELLING PARAMETERS

Due to the contradicting results in the cross-examination of the low-fidelity blades, it has been decided to systematically look at the effect of turbulence models, grid topologies and the effect of elasticity onto the here shown results. The focus is laid especially on the ONERA optimized blade and its performance in contrast to the HART-II rotor. The ONERA blade has been chosen as it deteriorates the most in ONERA's CFD simulations, but also showed the least improvement among the other low-fidelity blades when cross-examined by the other partners.

6.1. Effect of Turbulence Models

Comparative studies of various turbulence models are carried out by DLR and ONERA. Besides the already shown SA-R results with laminar-turbulent transition prediction and fully turbulent Menter SST results, additional simulations are carried with the Kok k-ω turbulence model, as well as laminar-turbulent transition prediction results with the Menter SST model on the given DLR grid setup.

In Figure 25, the results computed by DLR for the reference blade are shown, while in Figure 26 the results computed by DLR for ONERA's low-fidelity optimized blade are shown. For both rotors, the Kok k-ω delivers the lowest curves, while the Menter-SST model with laminar-turbulent transition prediction the highest curves. The spread of the Figure of Merit at design thrust for the HART-II rotor is 3.8% and 6.1% for the ONERA blade, which is considered a noteworthy gap. Yet, looking at the fully turbulent results of the two equations models (Kok k-ω FT and Menter SST FT), these gaps reduce to 1.2% and 1.8%.

This work is licensed under the Creative Commons Attribution International License (CC BY). Copyright © 2021 by author(s).

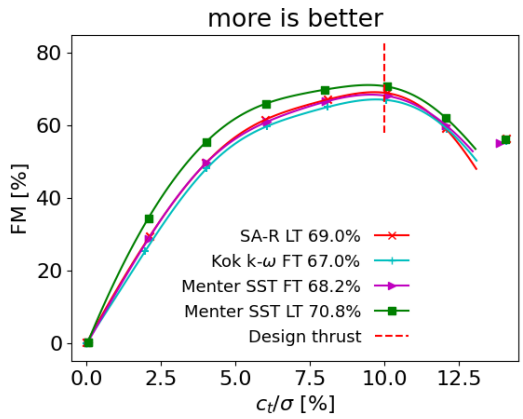

Figure 25: Figure of Merit polars of the HART-II for different turbulence modelling strategies using DLR's CFD approach.

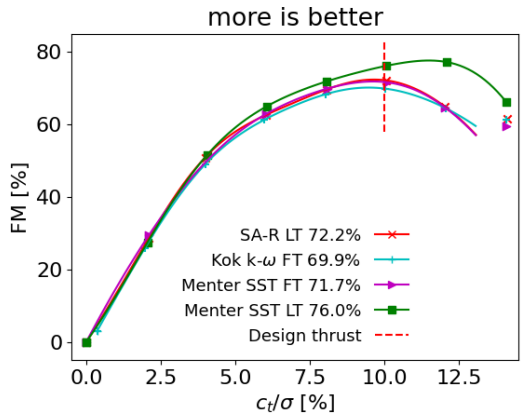

Figure 26: Figure of Merit polars of the Low-Fidelity optimized blade by ONERA for different turbulence modelling strategies using DLR's CFD approach.

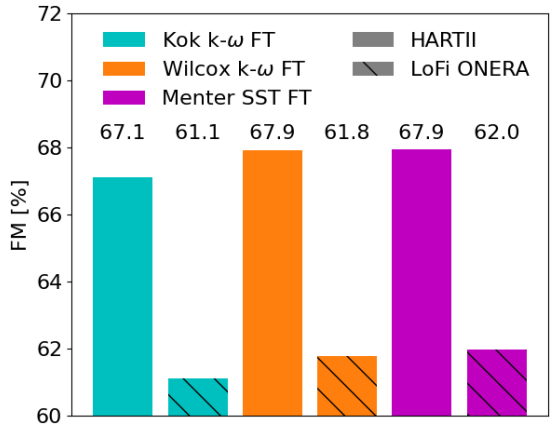

Figure 27: Figure of Merits @ design thrust with different turbulence models for the ONERA CFD setup.

ONERA also carried out a study of varying turbulence models for the two rotors, for which the reported Figure of Merit at design thrust is visualized in Figure 27. A similar tendency as for DLR is observed, the Kok k-ω model yields overall smaller Figure of Merits, whereas the Menter SST delivers higher Figure of Merits, therefore being a consistent observation. However, opposing to DLR, the low-fidelity optimized blade deteriorates noticeable for all turbulence models employed by ONERA over the reference blade. The difference between the models is 0.8% and 0.9%.

Since the turbulence model mostly influences the viscous effects, the skin friction distribution of the HART-II rotor is plotted in Figure 28. For the DLR results, the onsets of separation caused by the high upwash velocities induced by the tip vortex of the preceding blade are seen, which is most pronounced for the SA-R LT settings and shortly before separation for the Menter SST LT setting. On the suction side, the SA-R LT has the overall smallest skin friction. While the SA-R LT and Menter SST LT the location of the pressure side transition is roughly at the same location x/c ≈ 80%, only the SST model shows a reduction in skin friction for this location. This is somewhat surprising, since the application of laminar and turbulent regions is handled through an intermittency factor in DLR's FLOWer code, which is zero for laminar regions, and one for turbulent regions. Independently of the turbulence model, this intermittency factor is multiplied with the turbulent viscosity applied to the main equations and ultimately being responsible for the skin friction.

Opposing this, the Kok k-ω model has the most overall skin friction and thus delivers the smallest Figure of Merit at design thrust. Albeit these results, the strong deterioration as observed by ONERA for the low-fidelity blade optimized by ONERA cannot be purely explained by the effect of the turbulence models and only a small tendency can be attributed to using the Kok k-ω model over different turbulence models. The laminar-turbulent transition prediction has a more severe impact.

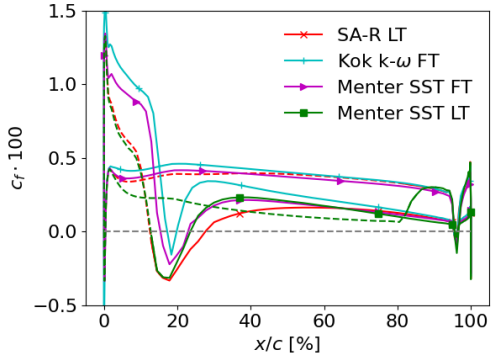

Figure 28: Skin friction distribution @ r/R =95% and design thrust for the HART-II rotor using various turbulent

This work is licensed under the Creative Commons Attribution International License (CC BY). Copyright © 2021 by author(s).

modelling strategies using DLR's CFD approach. Dashed lines mark laminar regions.

6.2. Elasticity

A rather brief section is dedicated to the different elastic modeling approaches. Imiela [49], [50] shows in his work the importance of incorporating fluid-structure coupling in the rotor blade optimization for rotors of similar size as in this study. Stanger at al. [51] demonstrate that the way to obtain new structural-dynamic properties for a new aerodynamic shape can have a noticeable effect on the performance, while Desvigne et al. [52] probably have the yet most advanced approach to update the structural layout of the blade with respect to geometric changes aimed at improving the aerodynamics of a rotor blade.

For the HART-II blade, the effect of neglecting elasticity in this flight condition is small, as can be deducted from the Figure of Merit polar Figure 29. The variation is below the effect of varying the turbulence model. The reason why the elastic blade has a better Figure of Merit at design thrust is that the structural torsion at the tip is about 1.2˚ for the DLR simulation and 0.6˚ for the ONERA simulations.

Looking at the other designs investigated in this paper, the torsional deformation and the final blade pitch are plotted in Figure 30. Most blades feature a fairly similar deformation to the HART-II blade except DLR's CFD optimized blade. For the similarly deformed blades it may be assumed that the effect leads to mostly a shift between the rigid and elastic simulations of the FM polar analogue to the HART-II blade.

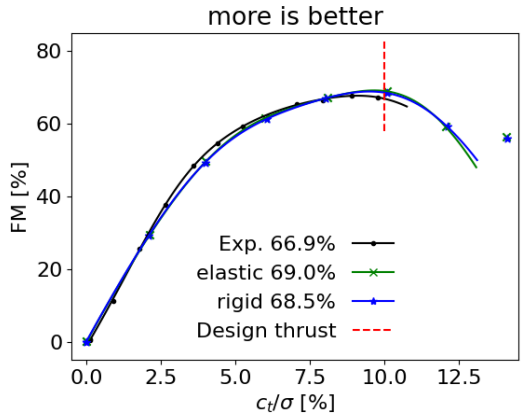

Figure 29: Figure of Merit polars for rigidly and elastically modelled HART-II blade computed by DLR's CFD approach (SA-R LT).

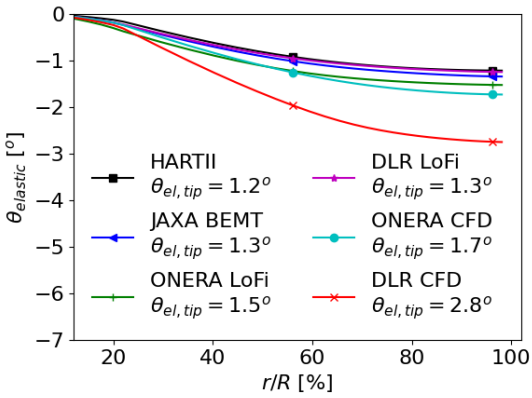

Figure 30: Torsional deformation for investigated blades using DLR's CFD simulation (SA-R LT).

6.3. Grid Topologies

Since the effect of the turbulence and elastic modelling cannot solely explain the contradiction of the CFD results for the low-fidelity blade optimized by ONERA, the effect of the grid is investigated. Thus, DLR has simulated the ONERA blade grids for the HART-II and the low-fidelity optimized grid and mimicking the CFD settings as close as possible with the ONERA CFD settings, namely using 2nd order JST scheme and Kok k-ω turbulence model in fully turbulent mode. Another Chimera setup is also established by DLR, which consists of 8 million grids points.

The comparison for the HART-II blade is given in Figure 31 and for the low-fidelity optimized ONERA blade in Figure 32. While for the HART-II rotor the results align well with minor variations, the results for the optimized blade clearly show the culprit for the discrepancies observed earlier. The ONERA and DLR solvers report a similar deterioration of the optimized blade when using the ONERA grid and settings, whereas the DLR monocoque and Chimera grid show a favorable behavior for this blade.

DLR repeated the exercise using the SA-R turbulence model without transition prediction on the ONERA grid, but with the application of the 4th order upwind scheme and found a drop in Figure of Merit from 70.0% for the HART-II blade to 61.0% for the low-fidelity optimized ONERA blade, additionally underlining the grid effect. Doing this on the DLR chimera setup yields numbers of 68.5% and 67.5% for the HART-II and ONERA low-fidelity optimized blade, respectively.

This work is licensed under the Creative Commons Attribution International License (CC BY). Copyright © 2021 by author(s).

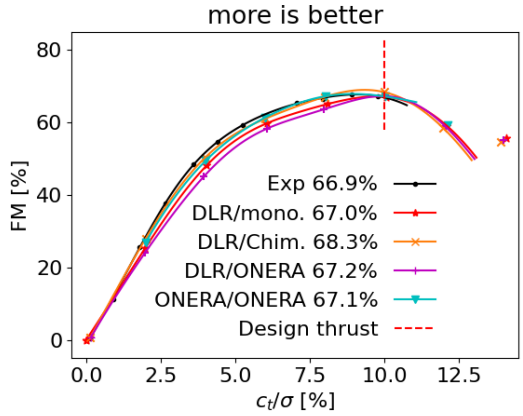

Figure 31: Figure of Merit polars for the HART-II rotor using different solvers and grids (DLR/mono. = DLR solver and DLR monocoque grid, DLR/Chim = DLR solver and Chimera setup, DLR/ONERA = DLR solver and ONERA grid, ONERA/ONERA = ONERA solver and grid)

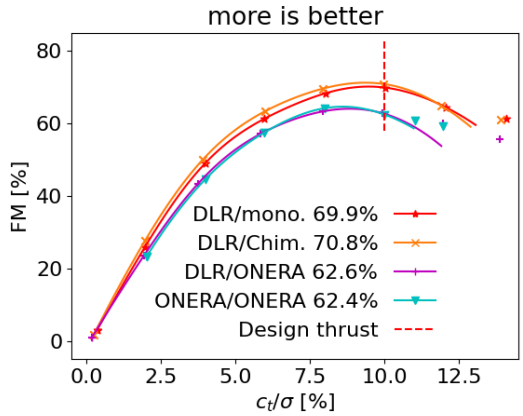

Figure 32: Figure of Merit polars for the low-fidelity optimized ONERA blade using different solvers and grids (DLR/DLR = DLR solver and DLR grid, ONERA/ONERA = ONERA solver and grid)

The conclusion from these studies is that the grid has a greater impact than the turbulence models or blade elasticity. Around $c_T/\sigma = 0.1$ the first signs of a stall can occur. At this point, the previous tip vortex may trigger stall and it is a matter not only of the employed spatial order, but also of the grid setup on how this is perceived. In Figure 33, the vorticity in the plane of the rotor is shown for the monocoque and the Chimera setup by DLR using the same numerical settings. The vortex strength is coincidentally almost the same for both grids, but the slightly skewed cells of the monocoque mesh alter the oncoming vortex shape slightly, thus delaying the stall at this point in combination with a slightly reduced blade flap. The flap reduction, however, is also attributed to the grid. For the second and third tip vortex passages, the roundness is successively lost for the monocoque grid, while for the cylindrical background mesh with more evenly distributed cells, these vortices keep their shape better.

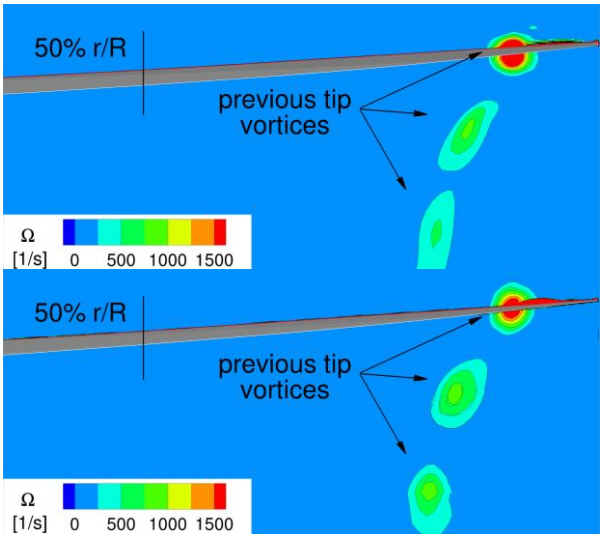

Figure 33: Vorticity plots. Sliced through the low-fidelity optimized blade by ONERA, viewed from behind the rotor. top: DLR's monocoque mesh, bottom: DLR's Chimera setup, Kok k-ω turbulence model, fully turbulent.

7. HIGH-FIDELITY OPTIMIZED BLADES

The chord and twist distributions of the CFD based optimizations are sketched in Figure 34 and Figure 35, respectively. JAXA has not performed a high-fidelity optimization, thus their low-fidelity blade is compared side by side with the CFD blades in this section. However, a previous study [1] by JAXA has shown a high correlation between BEMT based and CFD based optimization results, and it is expected that the blade geometry would not change significantly.

Similar trends are observed for chord and twist distributions obtained from low- and high-fidelity optimizations, that is chord reduction and increase of the twist at the blade tip (from r/R=0.8). However, the high-fidelity optimizations provide a smaller chord reduction and a higher twist at the tip with respect to the low-fidelity optimized blades as the high-fidelity blades try to avoid the stall phenomenon.

This work is licensed under the Creative Commons Attribution International License (CC BY). Copyright © 2021 by author(s).

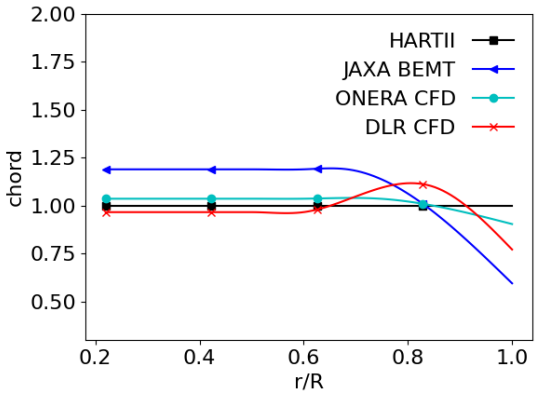

Figure 34: chord distribution of the CFD optimized blades.

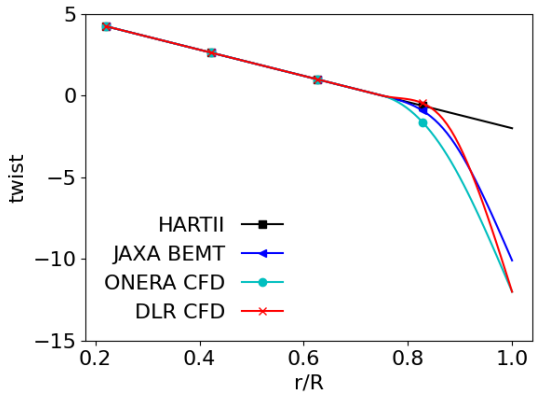

Figure 35: twist distribution of the CFD optimized blades.

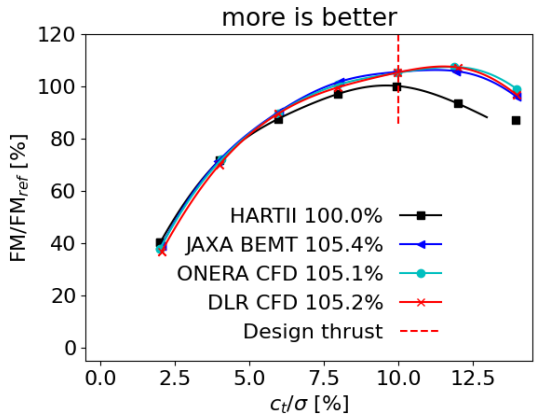

Figure 36: Figure of Merit polars for all CFD optimized blades computed by JAXA's CFD approach.

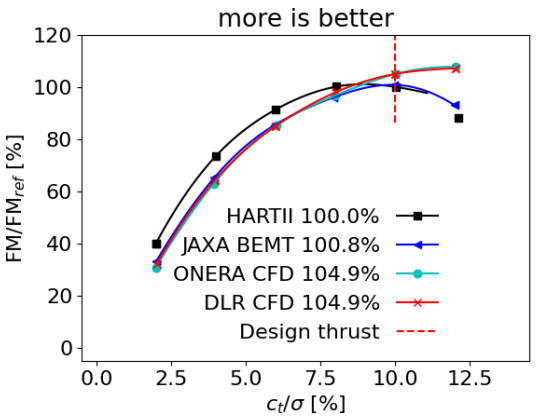

Figure 37: Figure of Merit polars for all CFD optimized blades computed by ONERA's CFD approach.

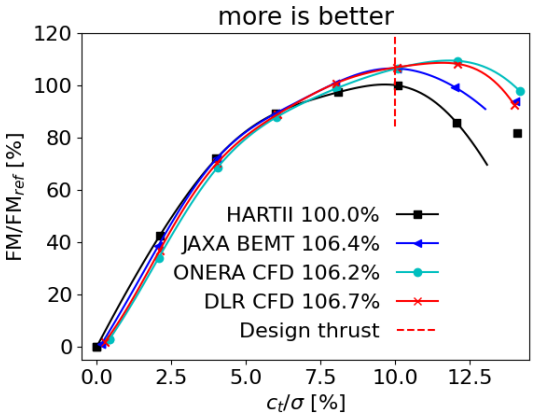

Figure 38: Figure of Merit polars for all CFD optimized blades computed by DLR's CFD approach (SA-R LT).

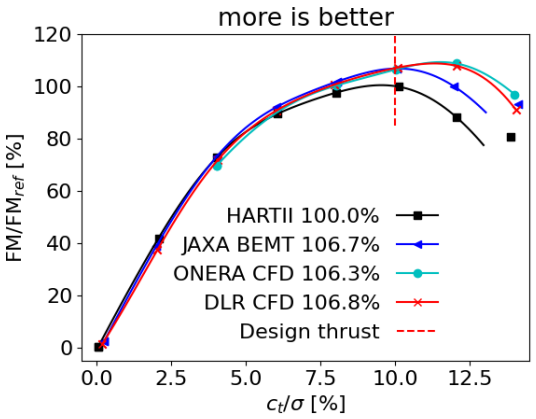

Figure 39: Figure of Merit polars for all CFD optimized blades computed by DLR's CFD approach (SST FT).

In Figure 36 to Figure 39 the cross-examined Figure of Merit polars of these blades are shown. Looking at JAXA's results, the BEMT optimized blade proves to be better than the CFD optimized blades, which

This work is licensed under the Creative Commons Attribution International License (CC BY). Copyright © 2021 by author(s).

comes a bit surprising. Moving onto ONERA's results, the pictures change and the two CFD optimized blades improve over the reference blade noticeable at the design thrust and above. In contrast to the other partners' results, the optimized blades show a reduced performance at thrusts below the design thrust. The DLR results show yet another tendency: Independently of the turbulence model setup, the DLR blade is the best, followed JAXA's low fidelity blade and last ranking is ONERA's CFD optimized blade when looking at the design thrust. However, at higher thrust, the CFD optimized blades prevail over the low fidelity optimized blade.

In order to understand the difference a bit better, the normal load distributions computed by each partner for each blade are given in Figure 40 to Figure 43. Again, little difference is seen for the two different turbulence modelling approaches for the DLR results. Comparing these with the ONERA results, the normal load distributions of the HART-II, JAXA BEMT and DLR CFD blades show a similar peak value, yet the ONERA blade has a lower peak for the DLR setups. Opposing this, JAXA's results feature slightly more triangular loads, mostly attributed to the fact of reduced vortex strength in the simulation. Here, the trend of the peaks aligns well with ONERA, as the peak of the ONERA and DLR blade are of similar magnitude for ONERA and JAXA.

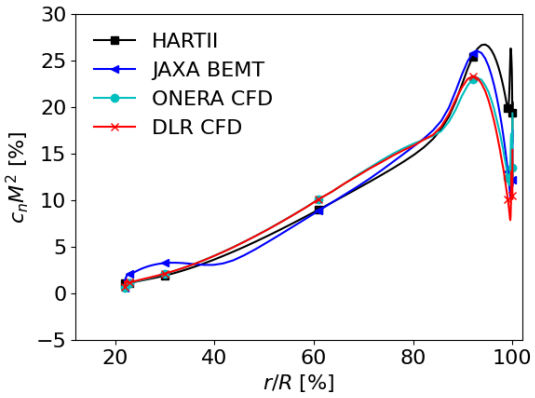

Figure 40: normal load distribution of all CFD optimized blades with JAXA's CFD approach at design thrust.

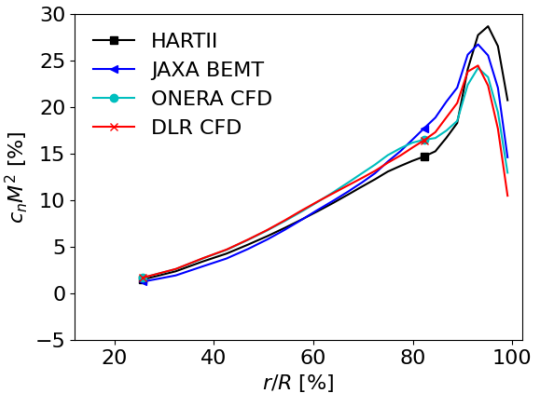

Figure 41: normal load distribution of all CFD optimized blades with ONERA's CFD approach at design thrust.

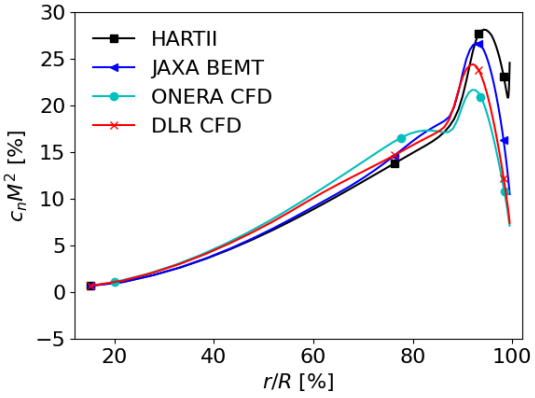

Figure 42: normal load distribution of all CFD optimized blades with DLR's (SA-R LT) CFD approach at design thrust.

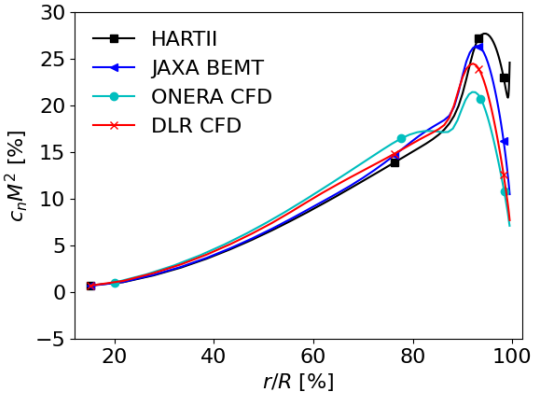

Figure 43: normal load distribution of all CFD optimized blades with DLR's CFD (SST FT) approach at design thrust.

Looking at the skin friction distributions for the outer r/R = 95% radial station for the different partners (Figure 44-Figure 47), the observed variation is

This work is licensed under the Creative Commons Attribution International License (CC BY). Copyright © 2021 by author(s).

greater than it is for the normal load distribution. For JAXA, the dip of the skin friction at x/c≈20% is given for the HART-II and JAXA blades, while for the ONERA and DLR blades it is almost not there. For the ONERA results, the dip predicted for the HART-II and JAXA blades correspond to losses in terms of pressure drag, which involves detached flow. In this regard, the DLR results coincide, as here also only the strong dips are resolved for the HART-II and JAXA blade, but not for the CFD optimized blades. For the SST FT results, these dips are less pronounced than for the SA-R LT results, matching the ONERA Kok k-ω results better.

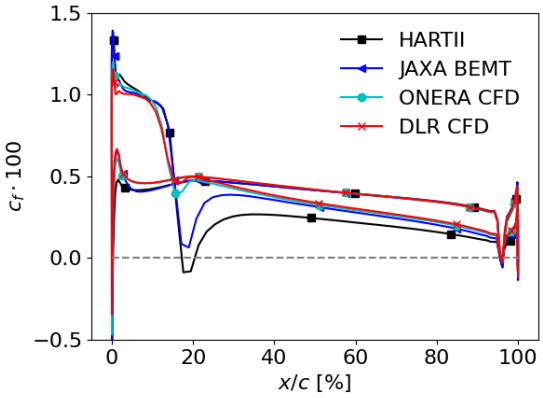

Figure 44: Skin friction distribution of all CFD optimized blades @ r/R = 95% and design thrust for JAXA's CFD simulations.

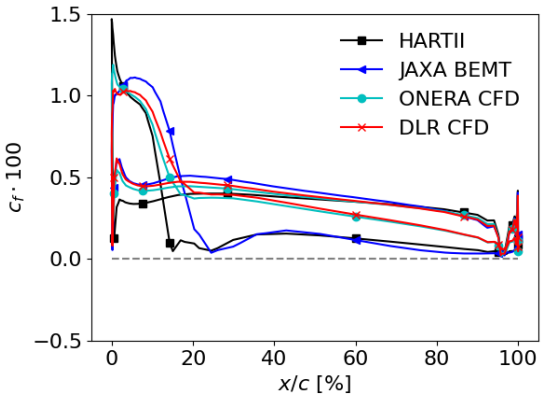

Figure 45: Skin friction distribution of all CFD optimized blades @ r/R = 95% and design thrust for ONERA's CFD simulations.

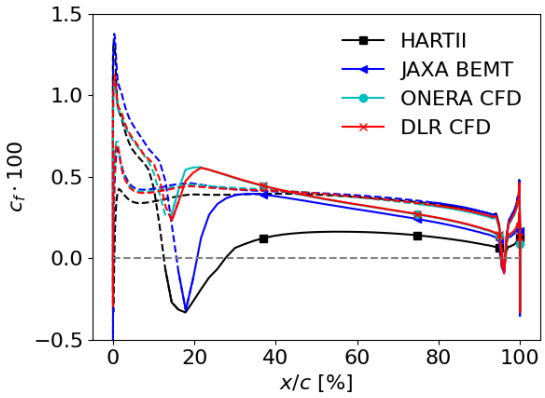

Figure 46: Skin friction distribution of all CFD optimized blades @ r/R = 95% and design thrust for DLR's CFD (SA-R LT) simulations. Dashed lines mark laminar regions.

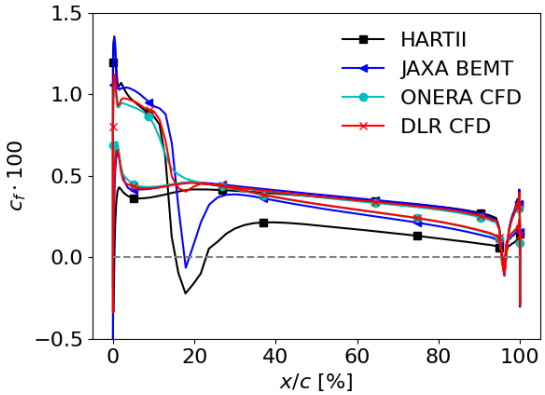

Figure 47: Skin friction distribution of all CFD optimized blades @ r/R = 95% and design thrust for DLR's CFD (SST FT) simulations.

While on the one hand this leads to a bit of inconclusive results, a certain commonality is observed though, as for JAXA and DLR all optimized blades improve by somewhere between 5-7% over the reference blade. Except for JAXA's low fidelity blade, this is also true for the ONERA results. Contrasting this with the previous lessons learned, a few contradictions can be resolved:

- JAXA has generally seen less severe separation effects due to a coarser background grid. This explains why the JAXA low fidelity optimized blade remains in good standing when cross-examined by JAXA with the other CFD optimized blades, even at higher thrusts.
- The ONERA grid has been more prone to induce (severe) separation, which then explains the little gain of the JAXA low fidelity blade over the reference rotor.

This work is licensed under the Creative Commons Attribution International License (CC BY). Copyright © 2021 by author(s).

- The DLR grid having slightly skewed cells delays the separation a little bit, but first signs are already visible for the HART-II and JAXA's low-fidelity optimized blade at design thrust. For higher thrusts, this separation becomes stronger and therefore the JAXA blade becomes worse than the other two CFD optimized blades at higher thrusts.

While this explains the general differences in the simulation results, it is safe to assume that CFD optimized blades are optimal even when compared by others. While the CFD optimized blades perform very similar with a similar twist distribution, the chord distribution is different indicating that these parameters have a lesser effect on the outcome.

To investigate this matter in more detail, the variable-fidelity surrogate models built from CFD data are visualized in Figure 48 and Figure 49 for ONERA and DLR, respectively. On top the $chord_1/chord_2$ parameter slice at the respective best blade is shown, while on the bottom the $\Delta\theta_1/\Delta\theta_2$ is seen. For ONERA's surrogate model the ONERA and DLR blades are within the plateau of the optimum of $chord_1/chord_2$ slice, while for DLR only little sensitivity with respect to chord parameters is observed. Looking at the twist surrogate model, which yields a similar plot as found in the previous JAXA-ONERA cooperation [3], a strong effect on the twist parameter is observed. Considering the knowledge of the grid sensitivity study, it becomes clear why the surrogate model from ONERA prefers a larger $chord_2$ parameter. For smaller $chord_2$ parameters, the likelihood of a separation on the outboard side increases (to due higher increased blade pitch) as is the case for JAXA's low-fidelity blade. Looking at the twist distribution, it would appear that JAXA's blade would be doing better if it had the ONERA chord distribution, since the slice is made at this parameter combination.

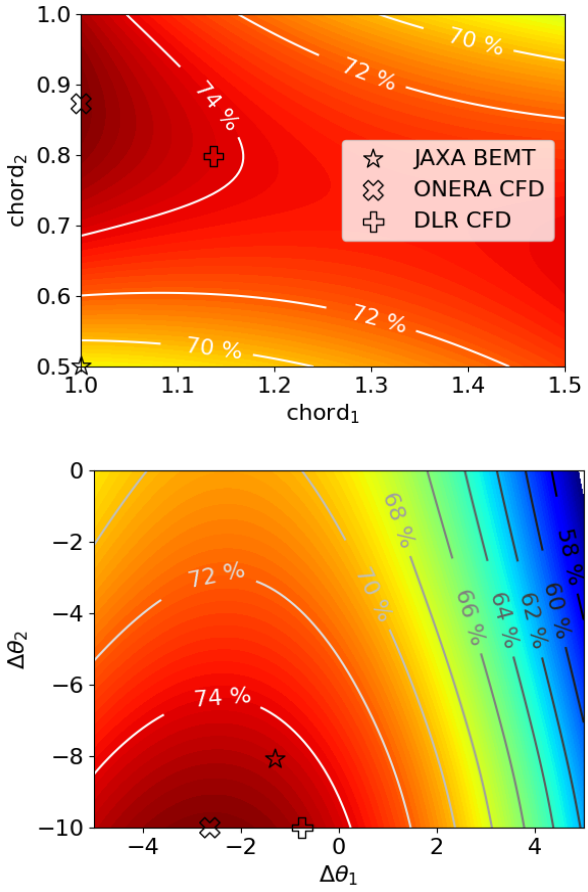

Figure 48: Figure of Merit contour plots of ONERA's surrogate model sliced through the best sampled rotor of DLR. Top: chord-plane, bottom twist-plane.

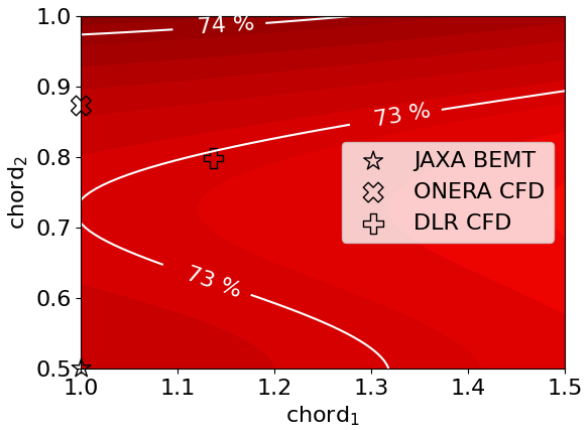

This work is licensed under the Creative Commons Attribution International License (CC BY). Copyright © 2021 by author(s).

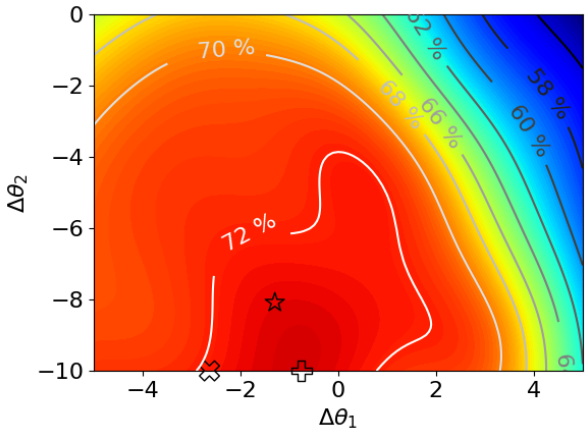

Figure 49: Figure of Merit contour plots of the DLR's surrogate model sliced through the best sampled rotor of DLR. Top: chord-plane, bottom twist-plane.

8. CONCLUSION & OUTLOOK

This paper concludes work package/phase I of the JAXA-ONERA-DLR cooperation on rotor optimization. The task was to optimize the HART-II blade for hovering flight by the current state-of-the-art methodologies by each research organization and compare the findings in order to harmonize tools and approaches. It was decided to utilize a rather simple parameterization that included three parameters for the chord distribution and two parameters for the twist distributions.

It was observed that for the baseline rotor, the low- as well as high-fidelity CFD simulations align well among partners. When re-evaluating the low-fidelity optimized blades from each partner with CFD based methods, discrepancies occur, which called upon a deeper investigation of the modelling approaches. The following conclusions from these side-studies are:

- The effect of turbulence modelling is roughly of the same order of including elasticity in the simulations and relatively small compared to the effect of the grid employed. While not directly investigated, the effect of the spatial numerical scheme seems to be negligible for the rotor performance.
- The effect on including the laminar-turbulent transition prediction is roughly of a similar magnitude than switching between SA-R, Kok k-ω, Wilcox k-ω and Menter SST. The differences of the turbulence models were greater on the DLR grid with less grid points than it was for ONERA's grid.
- The reason why elasticity plays a minor role is that the quarter chord axis remained unchanged with respect to the baseline rotor, therefore no additional levers have been introduced from anhedral or sweep. Therefore, care is advised to generalize this fact.
- The conservation of the tip vortex has a great impact on the performance prediction. JAXA employed a relatively coarse background grid and therefore resolved the weakest vortices, while the skewed cells of the periodic monocoque mesh without a background grid by DLR was also found modify the vortex shape.
- Cross-checking ONERA's grid with DLR tools revealed very similar results. Upon building their own Chimera setups, DLR was able to find similar trends as ONERA.

Through these studies, the outcome of the various results could be explained. Moving onto the high-fidelity optimization, the chance of separation found for these blades has been greatly reduced and thus all partners found similar improvements for the high-fidelity optimized blades. From the surrogate models of the high-fidelity optimizations it was also discovered that the alteration of blade twist has a significantly larger impact on the rotor performance than the alteration of the chord distribution.

A few guidelines are postulated here arising from the performed investigations for the design and optimization of helicopter rotor blades in hover:

- Low-fidelity tools based on the blade element momentum theory (BEMT) or finite state models should be applied cautiously. They do not include a tip vortex model and thus lead to false load predictions. The resulting designs, however, may still be useful if cross-validated with high-fidelity CFD.
- Performing efficient CFD simulations is a challenging task. While obviously including many grid points, elasticity, laminar-turbulent transition prediction are logically straightforward ways to improve the simulation fidelity, it is not trivial on what can be skipped to arrive at faster turnaround times.
    - With respect to the grid points, it was found that they need to be distributed correctly. The overset/Chimera interpolation requires similar cells, but also the background grid requires a certain resolution to capture at least the first tip vortex passage.
    - A monocoque periodic mesh will inherently have non-Cartesian cells. The cell skewness leads to distorted vortices. While highly efficient, these

This work is licensed under the Creative Commons Attribution International License (CC BY). Copyright © 2021 by author(s).

setups should be handled with care when employed near maximum Figure of Merit, because the outboard separation is triggered by the tip vortices of the previous blades.
- Elasticity may be excluded at first, if the quarter chord axis of the rotor remains untouched and airfoils are not changed.
- Laminar-transition prediction seems to have little effect on the rotor designs and can safely be skipped for planform or twist optimizations. Yet, in case for the empirical transition prediction of DLR, the added cost to include this is minimal and a noticeable impact on the absolute prediction values has been observed.

As seen from these studies, different tools and approaches may lead to different designs. Thus, it should be ensured that the optimum retrieved still operates well for slightly altered conditions and parameters, the cue being design robustness.

Overall, the first phase delivered many insights to all partners and therefore highlighting the importance of such a cooperation. Without having the comparison with others, the search for improvement becomes even more difficult and mistakes may remain undetected.

As an outlook, it is planned to investigate the HART-II rotor at a high advance ratio and reduced thrust requirements as required for compound helicopters. The research will again be purely dedicated to this flight condition to retrieve the individual best design. At a later phase it is planned to optimize the HART-II rotor at various flight conditions to obtain the aforementioned design robustness. The here found knowledge will be applied to further improve the respective simulations.

9. REFERENCES

[1] M. Sugiura, Y. Tanabe, H. Sugawara, and K. Takekawa, "Optimal Design of Rotor Blade for a Winged Compound Helicopter at High Advance Ratio," in *Proceedings of the 76th Annual Forum*, Virtual, 2020.

[2] G. Wilke, A. Länger-Möller, Y. Tanabe, Yasutada, M Sugiura, and H. Sugawara, "Tackling the HARTII test case: A joint effort by DLR and JAXA," in *6th Asian/Australian Rotorcraft Forum / Heli Japan 2017*, 2017.

[3] M. Sugiura, Y. Tanabe, T. Aoyama, B. Ortun and J. Bailly, "An ONERA/JAXA Co-operative Research on the Assessment of Aerodynamic Methods for the Optimization of Helicopter Rotor Blades, Phase II," in *42nd European Rotorcraft Forum*, 2016.

[4] W. R. Splettstößer, and B. G. van der Wall, and B. Junker, and K-J Schultz, and P. Beaumier, Y. Delrieux, and P. Leconte, and P. Crozier, "The ERATO Programme: Wind Tunnel Results and Proof of Design for an Aeroacoustically Ouptimized Rotor," in *25th European Rotorcraft Forum*, 1999.

[5] M. Wentrup, J. Yin, P. Kunze, T. Streit, J-H Wendisch, T. Schwarz, J-P Pinacho, K. Kicker, and R. Fukari, "An overview of DLR compound rotorcraft aerodynamics and aeroacoustics activities within the CleanSky2 NACOR Project," in *AHS Forum*, 2018.

[6] E. Fabiano, and D. Mavriplis, "Adjoint-Based Aeroacoustic Design-Optimization of Flexible Rotors in Forward Flight," *Journal of Americal Helicopter Society,* Vols. 62-4, pp. 1–17, 2017.

[7] L. Wang, B. Diskin, R. T. Biedron, E. J. Nielsen, and O. A. Bauchau, "Evaluation of High-Fidelity Multidisciplinary Sensitivity-Analysis Framework for Multipoint Rotorcraft Optimization," *Journal of Aircraft,* vol. 57, pp. 830–842, 2020.

[8] T. A. Fitzgibbon, "Advanced Rotor Blade Design based on High-Fidelity Computational Fluid Dynamics," 2021.

[9] G. Wilke, "Variable-Fidelity Methodology for the Aerodynamic Optimization of Helicopter Rotors," *AIAA Journal,* vol. 57, pp. 3145–3158, 2019.

[10] B. G. van der Wall, "A Comprehensive Rotary-Wing Data Base for Code Validation: The HART II International Workshop," *The Aeronautical Journal,* vol. 115, pp. 91–102, 2011.

[11] K. Kimura, M. Sugiura, Y. Tanabe, G. Wilke, and J. Bailly, "Cooperative research on rotor blade optimization between JAXA-ONERA-DLR: Results of Phase I," in *Fluid Mechanics Lecture / Aerospace Numerical Simulation Technology Symposium*, 2020.

[12] D. A. Peters, D. D. Boyd, and C. J. He, "Finite-State Induced-Flow Model for Rotors in Hover and Forward Flight," in *43rd Annual Forum of the American Helicopter Society*, 1987.

This work is licensed under the Creative Commons Attribution International License (CC BY). Copyright © 2021 by author(s).

[13] P.-M. Basset, O. Heuze, J. V. R. Prasad, and M. Hamers, "Finite State Rotor Induced Flow Model For Interferences and Ground Effect," in *57th Annual Forum of the American Helicopters Society*, 2001.

[14] B. Benoit, A.-M. Dequin, K. Kampa, W. von Grünhagen, P.-M. Basset, and B. Gimonet, "HOST, a General Helicopter Simulation Tool for Germany and France," in *56th Annual Forum of the American Helicopters Society*, Virginia, 2000.

[15] J. Bailly, B. Ortun, Y. Delrieux, Y. Mercier des Rochettes, "Recent Advances in Rotor Aerodynamic Optimization, Including Structural Data Update," *Journal of Americal Helicopter Society,* vol. 62, pp. 1–11, 2017.

[16] G. Wilke, "Quieter and Greener Rotorcraft: Concurrent Aerodynamic and Acoustic Optimization," *CEAS Aeronautical Journal,* vol. 12, pp. 495–508, 2021.

[17] Y. Tanabe, S. Saito, and H. Sugawara, "Validation of High Resolution CFD Analysis For Flowfield Around a Rotor," in *The 40th JSASS Annual Meeting*, 2009.

[18] L. Cambier, S. Heib, and S. Plot, "The Onera elsA CFD Software: Input from Research and Feedback from Industry," *Mechanics & Industry,* vol. 14, pp. 159–174, 2013.

[19] J. Raddatz, and J. K. Fassbender, "Block Structured Navier-Stokes Solver FLOWer," in *MEGAFLOW - Numerical Flow Simulation for Aircraft Design*, Berlin, 2005.

[20] S. Yamamoto and H. Daiguji, "Higher-Order-Accurate Upwind Schemes for Solving the Compressible Euler and Navier-Stokes Equations," Computers and Fluids, Vol.22, Nos.2-3, pp.259-270, 1993.

[21] E. Shima and K. Kitamura, "On AUSM-Family Scheme for All Speeds with Shock Detection for Carbuncle-Fix," Proceedings of 19th AIAA Computational Fluid Dynamics, AIAA paper 2009-3544, June 2009, 2009.

[22] A. Jameson, W. Schmidt, and E. Turkel, "Numerical Solution of the Euler Equations by Finite Volume Methods Using Runge-Kutta Time-Stepping Schemes," in *14th AIAA Fluid and Plasma Dynamics Conference*, 1981.

[23] G. Wilke, "New Results in Numerical and Experimental Fluid Mechanics," 1 ed., vol. XIII, Springer International Publishing, 2022 - accepted for publication, pp. 790.

[24] K. Kitamura, and E. Shima, "Towards shock-stable and accurate hypersonic heating computations: A new pressure flux for AUSM-family schemes," *Journal of Computational Physics,* vol. 245, pp. 62–83, 2013.

[25] S. Yoon, and A. Jameson, "Lower-upper Symmetric-Gauss-Seidel method for the Euler and Navier-Stokes equations," *AIAA Journal,* vol. 26, pp. 1025–1026, 1988.

[26] A. Jameson and T. J. Baker, "Solution of the Euler Equations for Complex Configuration," Proceedings of 6th Computational Fluid Dynamics Conference Danvers, AIAA paper 1983-1929, July 1983, 1983.

[27] R. Radespiel, C. Rossow, and R. C. Swanson, "Efficient cell-vertex multigrid scheme for the three-dimensional Navier-Stokes equations," *AIAA Journal,* vol. 28, pp. 1464–1472, 1990.

[28] S. Allmaras, F. T. Johnson, and P. Spalart, "Modifications and clarifications for the implementation of the Spalart-Allmaras turbulence model," in *Seventh International Conference on Computational Fluid Dynamics (ICCFD7),*, Big, 2012.

[29] J. Dacles-Mariani, D. Kwak, and G. Zilliac, "On numerical errors and turbulence modeling in tip vortex flow prediction," *International Journal for Numerical Methods in Fluids,* vol. 30, pp. 65–82, 1999.

[30] J. C. Kok, "Resolving the Dependence on Freestream Values for the k- Turbulence Model," *AIAA Journal,* vol. 38, pp. 1292–1295, 2000.

[31] C. C. Heister, "A Method for Approximate Prediction of Laminar-Turbulent Transition on Helicopter Rotors," *Journal of the American Helicopter Society,* vol. 63, pp. 1–14, 7 2018.

[32] F. R. Menter , M. Kuntz , and R. Langtry , "Ten years of industrial experience with the SST turbulence model," *Heat and Mass Transfer,* vol. 4, pp. 625–633, 2003.

[33] H. Yeo, M. Potsdam, and R. Ormiston, "Application of CFD/CSD to Rotor Aeroelastic Stability in Forward Flight," in *66th Annual Forum of the American Helicopters Society*, 2010.

[34] cadence, "The Choice for CFD Meshing," [Online]. Available: http://www.pointwise.com/. [Accessed 7 7 2021].

This work is licensed under the Creative Commons Attribution International License (CC BY). Copyright © 2021 by author(s).

[35] D. Maruyama, D. Bailly, and G. Carrier, "High-Quality Mesh Deformation Using Quaternions for Orthogonality Preservation," *AIAA Journal,* vol. 52, pp. 2712–2729, 2014.

[36] C. Benoit, S. Péron, and S. Landier, "Cassiopee: A CFD pre- and post-processing tool," *Aerospace Science and Technology,* vol. 45, pp. 272–283, 2015.

[37] C. B. Allen, "CHIMERA volume grid generation within the EROS code," *Proceedings of the Institution of Mechanical Engineers, Part G: Journal of Aerospace Engineering,* vol. 214, pp. 125–140, 2000.

[38] D. R. Jones, M. Schonlau, and W. J. Welch, "Efficient Global Optimization of Expensive Black-Box Functions," *Journal of Global Optimization,* vol. 13, pp. 455–492, 1998.

[39] M. Kanazaki, S. Jeong, and K. Yamamoto, "High-Lift System Optimization Based on the Kriging Model Using a High-Fidelity Flow Solver," *Transactions of the Japan Society for Aeronautical and Space Sciences,* vol. 49, pp. 169–174, 2006.

[40] M. Kanazaki, Y. Yokokawa, M. Murayama, T. Ito, S. Jeong, and K. Yamamoto, "Nacelle Chine Installation Based on Wind-Tunnel Test Using Efficient Global Optimization," *Transactions of the Japan Society for Aeronautical and Space Sciences,* vol. 51, pp. 146–150, 2008.

[41] J. Bailly, and D. Bailly, "Multifidelity Aerodynamic Optimization of a Helicopter Rotor Blade," *AIAA Journal,* vol. 57, pp. 3132–3144, 8 2019.

[42] M. C. Kennedy, and A. O'Hagan, "Predicting the output from a complex computer code when fast approximations are available," *Biometrika,* vol. 87, pp. 1–13, 2000.

[43] Z.-H. Han, and S. Görtz, "A Hierarchical Kriging Model for Variable-Fidelity Surrogate Modeling," *AIAA Journal,* Vols. 50-9, pp. 1885–1896, 2012.

[44] S. Takeda, M. Sugiura, Y. Tanabe, H. Sugawara, M. Kanazaki, and M. Harigae, "Influence of Pre-twist Distribution at the Rotor Blade Tip on Performance during Hovering Flight," *Transactions of the Japan Society for Aeronautical and Space Sciences,* vol. 58, pp. 39–44, 2015.

[45] M. Sugiura, Y. Tanabe, H. Sugawara, and M. Kanazaki, "Computationally Efficient and High Fidelity Optimization of Rotor Blade Geometry," in *40th European Rotorcraft Forum*, 2014.

[46] R. Storn, and K. Price, "Differential Evolution - A simple and efficient adaptive scheme for global optimization over continuous spaces," *Journal of Global Optimization,* vol. 11, pp. 341–359, 1997.

[47] J. A. Nelder, and R. Mead, "A simplex function for minimization," *Computer Journal,* Vols. 8-1, pp. 308–313, 1965.

[48] P. Küfmann, R. Bartels, B. G. van der Wall, O. Schneider, H. Holthusen, J. Gomes, and J. Postma, "The First Wind Tunnel Test of the DLR's Multiple Swashplate System: Test Procedure and Preliminary Results," in *AHS 72nd Annual Forum*, 2016.

[49] M. Imiela, "High-fidelity optimization framework for helicopter rotors," *Aerospace Science and Technology,* vol. 23, pp. 2–16, 2012.

[50] M. Imiela, "Mehrpunktoptimierung eines Hubschrauberrotors im Schwebe- und Vorwärtsflug unter Berücksichtigung der Fluid-Struktur-Wechselwirkung," 2012.

[51] C. Stanger, M. Hollands, M. Kessler, and E. Krämer, "Adaptation of the Dynamic Rotor Blade Modelling in CAMRAD for Fluid-Structure Coupling within a Blade Design Process," in *18. DGLR-Fach-Symposium der STAB*, 2012.

[52] D. Desvigne, R. Coisnon, B. R. Michel, A. Thomas, J. P. Pinacho, E. Roca León, "Multi-Objective Industrial Optimization of High-Speed Helicopter Main Rotor Blades with Dynamically-Adapted Structural Properties," in *45th European Rotorcraft Forum*, 2019.

This work is licensed under the Creative Commons Attribution International License (CC BY). Copyright © 2021 by author(s).